Studying Elliptic Flow in High Centrality Pb-Pb Collisions using Proton Collision Background Fitting

Bachelor's Thesis
Half a Semester Full-Time, 15 credits
Date of Examination: June 8th

Author
Philip J. Fredholm

Supervisors
Vytautas Vislavicius
Peter Christiansen

Presented to the Faculty during
Spring of 2023

LUND
UNIVERSITY

Faculty of Science
Department of Physics
Division of Particle and Nuclear Physics

1 Abstract

In this report, the elliptic flow in high centrality Pb-Pb collisions is calculated using two particle correlations $v_2\{2\}$ but without any imposed separation in η with data taken from the ALICE experiment at CERN in 2015. Instead, measurements of the same correlations in proton-proton collisions is used as a background to account for non-flow effects and data is correlated between the time projection chamber and the forward multiplicity detectors in order to avoid intra-jet correlations. Results were possible to attain up to 80% centrality but beyond this point the fitting failed in what was likely due to a lack of statistics. The results seemed to agree well with previous computations on ALICE data.

2 Acknowledgements

I would like to thank my supervisors Vytautas Vislavicius and Peter Christiansen for their help during this project.

3 List of Abbreviations

- QCD - Quantum Chromodynamics
- QGP - Quark-Gluon Plasma
- ALICE - A Large Ion Collider Experiment
- TPC - Time Projection Chamber
- FMD - Forward Multiplicity Detector
- ITS - Inner Tracking System
- PDF - Probability Density Function
- RHS - Right Hand Side
- LHS - Left Hand Side
- pp-collisions - proton on proton collisions
- Pb-Pb collisions - lead on lead collisions
- TeV - Teraelectronvolt
- GeV - Gigaelectronvolt
- GB - Gigabyte
- MB - Megabyte

Contents

4 Introduction

4.1 The Underlying Theory of the Strong Force

To this day, there are four known fundamental forces of nature which are believed to govern everything that may be observed on Earth[1]. Out of the two most commonly directly observable in every-day settings, gravity and electromagnetism, only electromagnetism is included in what is known as the Standard Model of particle physics. This model is often simply referred to as the 'Standard Model'. The other two forces included in the Standard Model are the so called weak and strong force. These forces are not directly noticeable in an every day experience, but they certainly are noticeable indirectly as their effects are paramount for the microscopic description of matter. See Figure 1 for an overview of the particles the Standard Model contains.

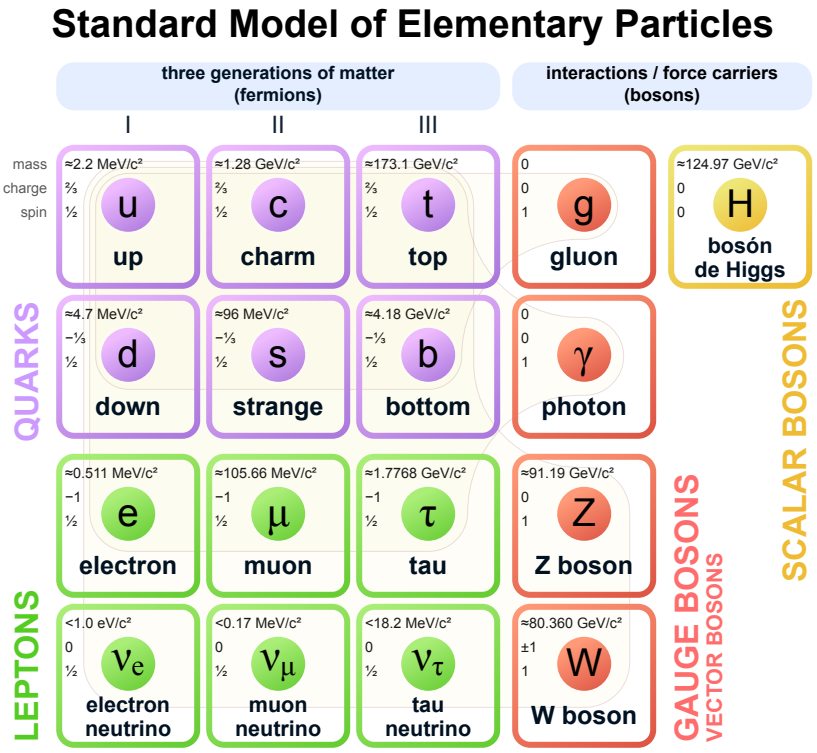

Figure 1: Shows the different particles of the Standard Model. The image was taken from Wikimedia Commons. Creator(s): MissMJ, Cush.

Out of the particles which form atoms, with electrons around a positively charged nucleus consisting of protons and neutrons, only the electrons are believed to be fundamental point particles. What is meant by 'point particles' is to say that they do not have any internal structure. The protons and neutrons are, on the other hand, believed to be built up of *quarks*.

[1]Some hypothesised concepts such as dark matter and dark energy are not fully explained by the Standard Model, c.f. chapter 22 of [1].

The quarks are unique in the way that they, and they alone, are the only massive particles which may interact via the strong force. The reason for stating that they are the only *massive* particles which interact with the strong force is technical, although very important to the discussion which will follow. Particles with electric charge are stated to 'couple to' the electromagnetic fields, which in turn are mediated by its own type of particle called a *photon*. Photons are well known to not interact with each other, which is not surprising considering that the classical limit of any quantum theory must give rise to superposition in classical electromagnetism. In the Standard Model, having them interact with each other would be tantamount to stating that they themselves carry electric charge. For the strong force, things are different. Much like the electromagnetic force, the strong force may be interpreted as being mediated through particles known as *gluons*. The difference here is that the gluons *do* carry the so called 'colour charge', which is defined in analogy to electric charge in electromagnetism. This colour charge is also carried by the quarks. Note that since quarks always carry colour charge, and since gluons may be emitted from quarks while also themselves carrying colour charge, it follows logically that gluons must carry both a colour charge and an anti-colour charge for global colour conservation to hold. Hence, the colour charge of an individual quark is not conserved as it changes when gluons are emitted. Interestingly, there are three possible 'colours' of quarks, red, green, and blue and eight different types of gluons to mediate these colours. The sum of particles with one of the red charge, one of the blue charge, and one of the green charge is said to be 'white' and being colour neutral. The word 'colour' is used only in analogy, but serves a useful purpose as i.e. red and blue are considered to form the colour 'anti-green' as it and the green colour cancel each other out. Furthermore, anti-particles do not carry colour but are instead viewed as having anti-colour which means that colour is conserved in pair production of quarks.

What makes *the strong force* strong has to do with that the gluons themselves carry colour charge. This means that the force carriers interact with each other. In classical electromagnetism, the strength of the Coulomb potential is inversely proportional to the separation between charges. This is often represented graphically as field lines of electrically charged particles being drawn further and further apart the greater the separation between particle becomes. With the strong force, the field lines are instead collimated into so called 'flux tubes' between particles in which the density of field lines does not decrease with distance. This leads to an effect commonly known as *asymptotic freedom*. See Figure 2 for an illustration and please note that this figure took inspiration from Figure 17.2 in [1]. In fact, the strong force is much like that of a spring in that it increases the greater the separation is. However, in this quantum-case things are somewhat different. Once the 'spring' is stretched enough, the energy stored in the field eventually becomes so great that it may be energetically favourable to pair produce new quarks in-between the original ones, thus decreasing the colour separation. This effect leads to that quarks are not possible to observe on their own, and only in colour neutral combinations. In the white combinations, the charges screen each other. This is known as 'colour confinement'. The asymptotic freedom means that the particles are more 'free' and less impacted by the strong force the closer they are together, unlike for example the case of Newton's law of gravitation where the force becomes smaller for greater separations.

One special consequence of colour confinement are so called jets. If quarks are separated and still have a lot of kinetic energy, many more quarks will end up being pair produced when

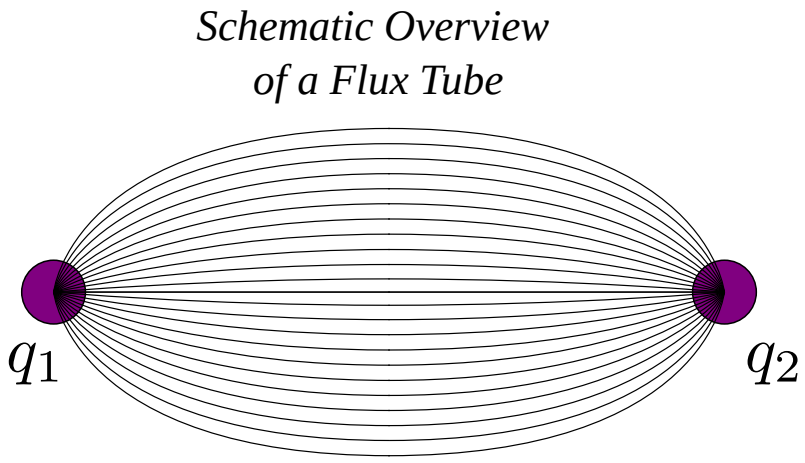

Figure 2: Shows a simplified illustration of imagined field lines for the strong force becoming collimated due to the gluon-gluon interaction. Please note that this illustration took inspiration from Figure 17.2 in [1].

more and more flux tubes end up broken. Since the initial momentum will be conserved, such beams of quarks will be very collimated and result in many particles 'flying off' in the same direction. Usually these jets appear in pairs of two going in opposite directions to conserve momentum, but three jet events are also possible if i.e. gluons are radiated leading to another jet. See chapter 7.2 of [2]. In the case of two jets, these are often said to be 'back to back' (at least in their centre of momentum frame) since, due to momentum conservation, there is an azimuthal angle of approximately π between them.

Composite particles of quarks are called *hadrons*, and with the exception of very exotic matter, hadrons come in two types. The first type is the *baryon*, which consist of colour-neutral bound states of three quarks. The other type is made up of *mesons*, which consist of bound states of a quark and an anti-quark. Anti-quarks carry anti-colour charge so the meson as a whole is white. It is important to keep in mind that due to the quantum nature of such systems, and due to the 'sea' of virtual particles like gluons coming in and out of existence, a hadron is not strictly e.g. red and anti-red, but a superposition of all possible states. Also keep in mind that gluons exchanging colour charge also have colour charge which makes the situation more complicated. Finally, it should be mentioned that the full description of the strong force is given by the so called theory of *quantum chromodynamics*, which is often abbreviated as 'QCD'. In QCD, the differently coloured quarks form a triplet under an $SU(3)$ rotation. The gluon fields are derived from demanding a local gauge invariance under rotations in this 'colour space' since it should not matter which label, i.e. 'red', 'green' and 'blue', is attached to which physical state. See chapters 1 and 17 in [1].

For a more detailed overlook of the Standard Model and its Lagrangian, see chapters 1 to 7 and chapter 17, with particular focus on chapter 7.5 and chapter 7.6 in [1].

4.2 The Quark-Gluon Plasma

While the concept of colour confinement certainly applies under present day conditions on Earth, it is possible that this has not always been the case everywhere in the Universe. If

matter becomes dense and hot enough, a phase transition occurs into a state known as a *quark-gluon plasma*, often denoted by 'QGP'. In the quark-gluon plasma, the density of colour charges (quarks and gluons) is so large everywhere that the net colour charge anywhere is practically white. Hence, there is no longer any reason for there to be any colour confinement and quarks may move more freely. In other words, the region where the asymptotic freedom 'gives freedom' is greatly increased. It turns out that this state of matter behaves very similar to a perfect fluid, see chapters 1 and 2 of [3].

This new state of matter is of interest to study as it has been hypothesised that the early Universe consisted of a QGP the first few moments after the Big Bang. It is also believed that a quark-gluon plasma may exist at the centre of neutron stars, see chapter 7.1.3 of [2]. Hence, if the Big Bang is to be fully understood, it is likely that the QGP too will have to be understood. Furthermore, studying the QGP also provides various ways to test theoretical models of QCD, which are almost never solvable analytically.

Additionally, it should be noted that as this might provide insight into the very early Universe, and hence the origins of everything, such insight could have important societal impacts. The role of such knowledge in society and the philosophy of science might also be impacted in future if the origins of the Universe would be understood.

One problem with producing a QGP on Earth is that the temperatures involved would lead to a very rapid cooling and expansion of the medium, so it would only exist for very brief amounts of time. The only way to produce and study a quark-gluon plasma today is through particle accelerators and particle detectors, respectively. The way to currently produce a QGP is with two beams of heavy ions[2] that are accelerated to relativistic speeds, where the kinetic energies per nucleon may be much higher than their rest energies, and then collided inside of a particle detector. Since the QGP only exists for a very brief amount of time, the only way to study it is to do so indirectly. One observation of its existence is the so called jet quenching, in which a single jet is detected instead of at least two. This is due to the quarks in the other jet having been absorbed by the very dense QGP. Other indications of the existence of the QGP relate to energy densities and other more technical calculations. See chapter 1 and 2 of [3] and Chapter 7.1.3 of [2].

4.3 The Detector Setup

A particle detector typically consists of multiple layers in a cylindrical shape around the beam line in which collisions happen. First and foremost, it is important to mention that detectors are typically surrounded by a magnet. Since powerful magnetic fields will bend the paths of moving charged particles, this allows for the charge to momentum ratio of particles to be figured out from curvatures of measured trajectories. The innermost parts of detectors are typically tracking detectors since these disturb the particles the least. In the ALICE (ALICE stands for 'A Large Ion Collider Experiment') detector, see [5], the main tracking detector for this analysis will be the so called *time projection chamber*, henceforth abbreviated as 'TPC', which is used to track the particles which come out of a collision.

In order to measure the flow from a heavy ion collision, data from the TPC turns out to be important. The TPC covers almost the entire solid angle surrounding the collisions, and will

[2]There is actually an ongoing discussion about detecting elliptic flow in proton on proton collisions, c.f. [4].

thus give important information on the paths followed by the particles. The working principle of a time projection chamber is mostly that of drift tubes, although there are some important differences. The TPC, as seen in Figure 3, is split down the middle into two halves by a cathode-plane (which is at a voltage of -100 kV) such that there are two cylindrical regions. At the two ends of the cylindrical TPC, the disks are segmented into trapezoidal regions, as is hinted by the support beams which are visible in Figure 3. Inside these trapezoidal regions there are so called readout chambers in which the anodes are located. Unlike the case of the Geiger-Müeller tube where there is only one wire, there are multiple wires inside these readout chambers in order to give spatial information of where the particles end up. In between these regions, a gas is present. When charged particles pass through this gas, they ionise particles. While a recombination would typically happen in the absence of the electric potential, its presence will cause the charged particles to begin to drift towards their respective electrodes. While these ionised particles in turn ionise even more particles in a so called 'Townsend Avalanche', the voltage of the TPC is such that it is in *proportional region* and not in the Geiger-Müeller region. That is to say that the charge collected at the electrodes is proportional to the initial amount of energy deposited by the ionising particles. Depending on where and when the different electrodes detect charge, the path of the particles in the xy-plane may be determined. Complementing this information with that the drift velocity of the particles inside the TPC is known, the full three-dimensional path may be deduced. See chapter 4.4 of [2], [6] and chapter 3.2 of [5]. Note that the TPC is much more complicated than this basic explanation, see [6] and chapter 3.2 of [5] for a more in-depth explanation. The TPC, along with other detectors, may be seen in Figure 3. Another important part

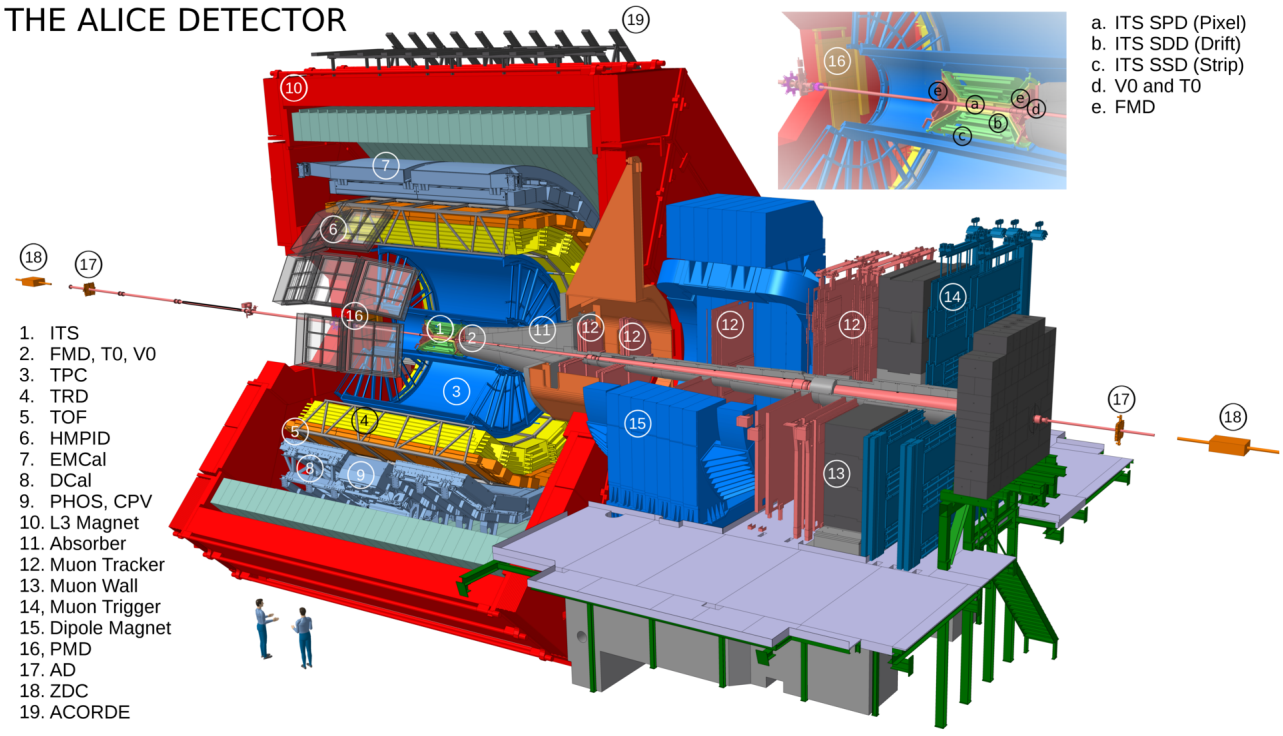

Figure 3: Shows an overview of the ALICE detector and its various parts. This image was taken from CERN's website. Credit: CERN, Arturo Tauro.

of the ALICE detector for this analysis are the so called forward multiplicity detectors, often abbreviated as 'FMDs's. These serve the purpose to measure how particles go close to the beam lines, as this is a 'blind spot' to the TPC. These simply count how many particles go within a certain direction along both the forward and backwards path close to the beam line. [7]. See chapters 1 and 2 of [3]. The FMD:s are so called *silicon strip detectors*. The operating principle of theses is using the band gaps in silicon, along with doping, to create a depletion region. When charged particles pass through this region they may excite electrons across the band gap, resulting in free charge carriers in the form of electrons and holes. These will then start to move due to the electric field in the depletion region, resulting in a measurable current. If many such small depletion regions are placed close to each other, the location of a particle and its path may be deduced. See chapter 4.6.2 of [8]. The actual FMD:s then consist of rings of segmented silicon rings, see chapter 5.3 of [5] and Figure 4.

Finally, another detector that is of relevance should be mentioned. The so called *inner*

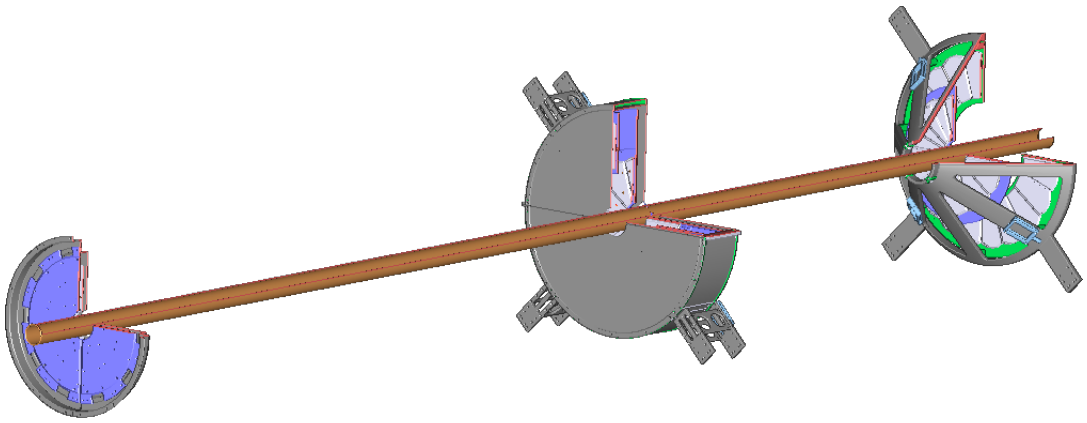

Figure 4: Shows a sketch of the various segmented silicon rings used in the FMD:s around the beam line. This image was created by Christian Holm Christensen, NBI

tracking system, abbreviated as 'ITS', also uses silicon technologies to detect particles. It uses both silicon strip detectors, as well as other silicon type detectors and is placed inside of the TPC as may be seen in Figure 3. The ITS has multiple purposes, and among them are determining primary and secondary particle interaction vertices as as well as to help improve the tracking in the TPC by providing additional information. See Chapter 3.1 of [5].

4.4 The Coordinate System

In order to quantify the geometry of a collision, a vector quantity **b** called *the impact vector* is typically introduced. It is defined as the distance between the centres of the colliding nuclei. See Figure 5 for an illustration of this. Note that nuclei are quantum-mechanical objects with substructures (which is to say that they are composite objects containing quarks) and are not actually spheres, and many heavy nuclei are often deformed (see chapter 2.5.2 of [9]) to the point where an ellipsoid might even provide a better approximation. However, the existence of magic numbers for nuclei should of course still be kept in mind as the existence of magic numbers means that heavy nuclei do not per se have to be deformed. The nuclei in Figure 5 are only portrayed as circles for illustrative purposes. The points O_1 and O_2

are the the centres of the colliding nuclei and $\mathbf{p}_1$ and $\mathbf{p}_2$ in the figure are their respective momenta. Another quantity called *the impact parameter* b is also usually introduced and is simply defined as the magnitude of the impact vector. See chapters 1 and 2 of [3].

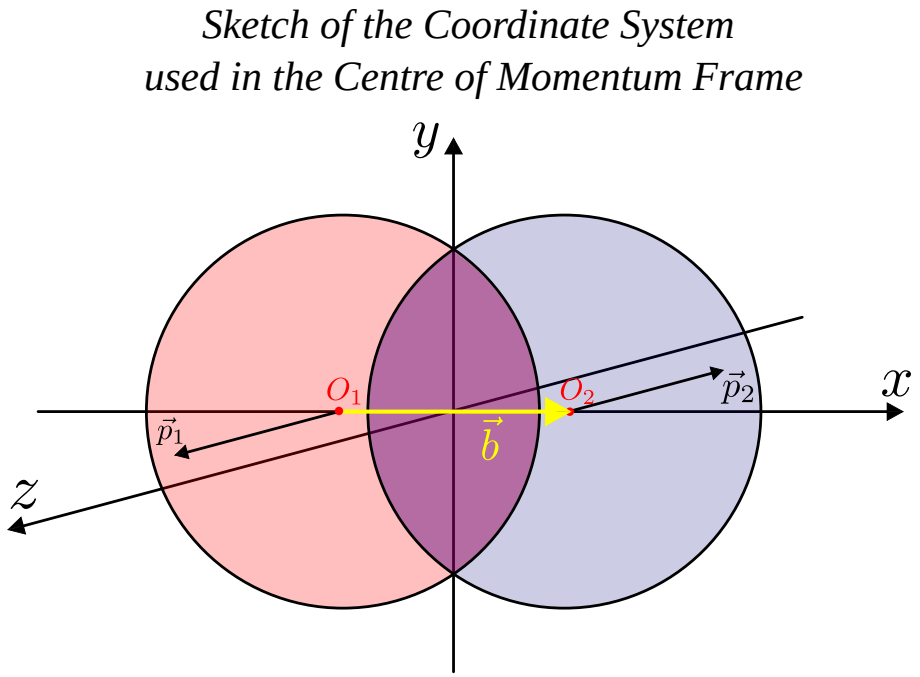

Figure 5: Shows an illustration of the definition of the impact parameter **b**. The quantities $\vec{p}_1$ and $\vec{p}_2$ (denoted are the respective momenta of the nuclei and O_1 and O_2 the positions of the centres. Please note that nuclei are not actually spheres and are only portrayed as circles for illustrative purposes.

Commonly, either a standard Cartesian coordinate system, a spherical one or a cylindrical one is used to make measurements. However, this is not the case with the data from the ALICE detector used for calculations in this project. The coordinate system used to collect data will be explained based on Figure 3 and Figure 6. As in a typical cylindrical coordinate system, the z-axis will be used as a coordinate along the beam line. While the x-axis is typically taken to be along the impact vector within an event, it will, in the laboratory frame, be taken as being perpendicular to the z-axis but still in the same horisontal plane as the z-axis. Furthermore, the x-axis will be taken to be in the horisontal direction such that the y axis may be taken as vertical while also making the coordinate system right handed. From this, the angle φ will be defined as the counter-clockwise angle in the xy-plane starting from the x-axis such that it serves as the azimuthal angle. This angle φ will then be taken as the second coordinate in addition to the z-coordinate which is taken in the same way as in cylindrical coordinates. The final coordinate used will be the *pseudorapidity* η, defined as

$$\eta = -\ln\left[\tan\left(\frac{\theta}{2}\right)\right] \tag{1}$$

where θ is defined as the counter-clockwise angle in the yz-plane starting from the z-axis in positive direction. Please note that θ is taken as a strictly positive quantity as the orientation will still be uniquely determined by the value of φ. See Figure 6 for an illustration.

The reason for using the coordinate η is that it is equal to another quantity called the *rapidity* for highly relativistic particles, which helps connecting theory and experiment. It should be noted that in the limit of $\theta \to 0$, $\eta \sim -\ln(0) \ -(-\infty) = \infty$), and that in the limit $\theta \to \pi$ one finds that $\eta \to -\ln(\tan(\pi/2)) = -\ln(\infty) = -\infty$. In-between these two extremes, for example at $\theta = \pi/2$, $\eta = -\ln(\tan(\pi/4)) = -\ln(1) = 0$. Hence, $\eta \in (-\infty, \infty)$ and, clearly, values of η corresponding to the positive z-direction are positive and values corresponding to negative z-direction are negative. See chapters 1 and 2 of [3].

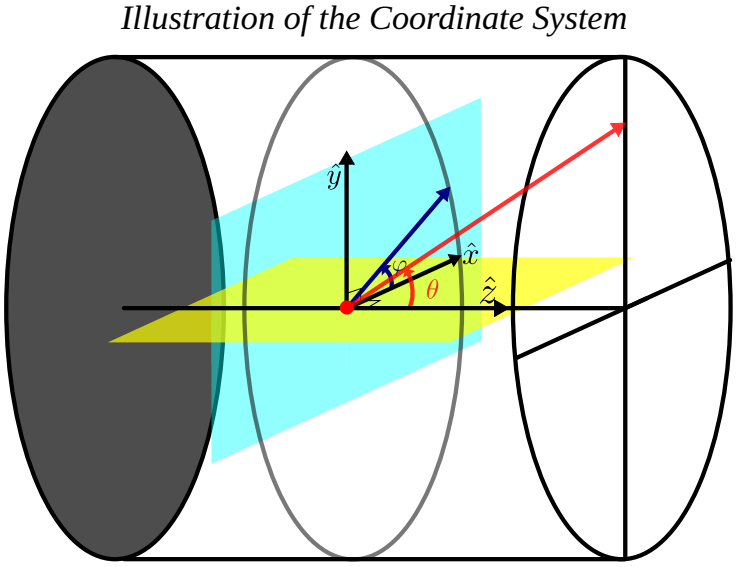

Figure 6: Illustrates how the coordinates φ and η are defined in relation to Cartesian and cylindrical coordinates.

4.5 The Definition of Centrality

While the impact parameter could be viewed as an ideal way to characterise a given collision, it is not always known. The issue with not knowing the impact vector is that the collision between the nuclei will take place at some angle φ, often denoted Ψ_{RP}, in the plane transverse to the beam line which will be important for the mathematical description of the collision in the next section. The value of Ψ_{RP} gives the so called *reaction plane*, which is spanned by the impact vector and the beam line vector $\hat{\mathbf{z}}$.

To experimentally measure the centrality, the so called V0-detector, which may be seen in Figure 3, is used. The category of detectors known as scintillation detectors, which the V0 detector belongs to, operates on the principle of charged particles exciting electrons in the medium it passes by. When these electrons are de-excited, so called scintillation light is emitted which may then be observed by photomultiplier tubes, see chapter 4.4.4 of [2]. Although the relationship between the number of particles produced in an heavy ion

collision and the centrality is complicated for several reasons such as secondary particles being produced after the collision, it may be determined (see section 5.4.1 of [5]) that the relationship between the number of primary particles in a collision and the measured signal is monotone. From this, the centrality may be deduced in a treatment which is beyond the scope of this report. For this project, the data was already available with the centrality calculated. Should the reader be interested in a more detailed overview, see [10].

4.6 Description through Flow Harmonics

To describe the 'flow' of particles 'flowing out' from the expanding QGP, a Fourier series is often used. This series has the form

$$f(\varphi) = 1 + \sum_{k=1}^{\infty} 2v_k \cos(k(\varphi - \Psi_{\mathrm{RP}})) \tag{2}$$

where Ψ_{RP} gives the reaction plane, φ is the angle and v_k are the so called *flow harmonics*. The Fourier series may be interpreted as being proportional to the number of particles 'flowing out' in a given φ direction. The reason for the Fourier series not containing any sine-functions is due to symmetry. The cosine functions are even with respect to Ψ_{RP} while sine functions are odd with respect to ditto. From Figure 5, it is clear that the initial geometry (even if the nuclei were approximated as ellipsoids instead of spheres) that the QGP, and hence its flow, is symmetric with respect to Ψ_{RP}. Hence, any term which does not display such a symmetry around may be omitted Ψ_{RP}. Clearly, this is only a one way implication as higher order terms which display this symmetry do not necessarily have to be non-zero. Furthermore, the term with v_1 is commonly omitted since in the case of $k = 1$, called *directed flow*, there is a net flow in a given direction. If the collisions are 'head on' in the laboratory frame, that is to say that the laboratory frame is the centre of momentum frame, conservation of transverse momentum would demand this term to be 0. Clearly, the higher order terms do not suffer from this problem.

While all flow harmonics are technically needed to characterise the flow, it is typical that the flow is characterised by v_2 which gives the so called *elliptic flow* which is commonly the dominating coefficient. Note that the flow could of course vary with η depending on where in the detector it is measured. Furthermore, the flow could of course be different for particles with different transverse momenta p_T and will obviously vary depending on the centrality of the collision. Finally, the asymmetry in momentum distribution is of course caused by the pressure gradients caused by the initial spatial asymmetry when nuclei collide, see i.e. Figure 2 in [11].

Measuring the different flow harmonics turns out to be important in order to describe the properties of the QGP medium. Since it is a medium, it is expected to have collective properties, and one such property would be the collective flow which is a process which the entire medium undergoes. Using a quantitative description of the quark-gluon plasma allows for a comparison to be made to the properties of the idealised *perfect fluid*, see chapter 2 of [3].

One property of the QGP which relates to it being a perfect fluid is the ratio of the so called shear viscosity to the entropy density, which has previously been found to be very close to the theoretical quantum mechanical lower limit [12]. Furthermore, the expansion of

the QGP as it begins to cool down almost entirely happens as relativistic hydrodynamics would predict. Additionally, it is also known that initial fluctuations are visible throughout the entire expansion (which turns out to be the origin of v_3 being non-zero). While statistical processes involving i.e. diffusion would indicate that such initial fluctuations are not important, this is not what has been observed previously. This may be taken as strong indication that there are very strong internal correlations which govern the QGP. [11] [12].

Furthermore, the very small shear viscosity can be showed to be associated with a very short mean free path. This relates back to the very strong correlations between particles in the QGP. [12]. Finally, it is even possible to show that signals may propagate at the speed of light through the QGP [11].

4.7 Theoretical Approach

The aim of this project is determine how particles flow out from the QGP in the φ-direction while studying proton on proton collisions to account for non-flow effects arising from QCD such as jets. If the reaction plane Ψ_{RP} was known, one could simply fit measured data to a Fourier series

$$f(\varphi) = 1 + \sum_{k=1}^{\infty} 2v_k \cos(k(\varphi - \Psi_{\mathrm{RP}})), \tag{3}$$

which gives how many particles flow out in each direction, and then determine the elliptic flow v_2 from it. One way to do this would be to fit the data to this function. Another approach is to derive the formula

$$\left\langle \cos(k(\phi_{\mathrm{tracks}} - \Psi_{\mathrm{RP}})) \right\rangle = v_k, \tag{4}$$

where the brackets denotes taking the expectation value. The notation has been changed from φ to ϕ to denote that this expectation value is over the measured values of the angle φ and not over an isotropic distribution of values. To understand why this equality holds, one should first note that equation (3) must be linearly proportional to a probability density function (PDF) of the distribution of particles 'flowing out' from the QGP. Since the expectation value is defined as

$$\langle x \rangle = \sum_i p_i x_i \tag{5}$$

where x_i are the measured values and p_i the probability of measuring that value, it follows that in the limit of an unlimited supply of particles flowing out,

$$\left\langle \cos(k(\phi_{\mathrm{measured}} - \Psi_{\mathrm{RP}})) \right\rangle \propto \sum_i \Big(\mathrm{d}\phi \; f(\phi) \Big) \cos(k(\phi - \Psi))) = \int_0^{2\pi} \mathrm{d}\phi f(\phi) \cos(k(\phi - \Psi)) \tag{6}$$

where subscripts on ϕ and Ψ have been dropped to clean up the notation. To restore a full equality, the RHS simply needs to be divided by the proper normalisation factor for $f(\varphi)$.

Doing this, and using the orthogonality of the cosines, it is found that

$$\left\langle \cos(k(\phi_{\text{measured}} - \Psi_{\text{RP}}))\right\rangle = \frac{\int_0^{2\pi} \mathrm{d}\phi f(\phi)\cos(k(\phi-\Psi))}{\int_0^{2\pi}\mathrm{d}\phi f(\phi)} \tag{7}$$

$$= \frac{\int_0^{2\pi}\mathrm{d}\phi\left(1+\sum_{k=1}^{\infty}2v_k\cos(k(\phi-\Psi))\right)\cos(k(\phi-\Psi))}{\int_0^{2\pi}\mathrm{d}\phi\left(1+\sum_{k=1}^{\infty}2v_k\cos(k(\phi-\Psi))\right)} \tag{8}$$

$$= \frac{2v_k\int_0^{2\pi}\mathrm{d}\phi\cos^2(k(\phi-\Psi))}{2\pi}. \tag{9}$$

All terms with cosines have vanished in the denominator since since they all integrate to 0 over a full period (note that k is an integer). In the numerator, the orthogonality of cosines has been used to set all terms but one to 0. To continue, the double angle formula for cosines $\cos(2\theta) = 2\cos^2(\theta) - 1$ will be used in reverse to find

$$\left\langle \cos(k(\phi_{\text{measured}} - \Psi_{\text{RP}}))\right\rangle = \frac{2v_k\int_0^{2\pi}\mathrm{d}\phi\cos^2(k(\phi-\Psi))}{2\pi} \tag{10}$$

$$= \frac{v_k}{\pi}\int_0^{2\pi}\mathrm{d}\phi\left(\frac{1}{2}+\frac{1}{2}\cos(2k(\phi-\Psi))\right) \tag{11}$$

$$= \frac{v_k}{2\pi}\int_0^{2\pi}\mathrm{d}\phi\left(1+\cos(2k(\phi-\Psi))\right) \tag{12}$$

$$= \frac{v_k}{2\pi}\int_0^{2\pi}\mathrm{d}\phi = v_k. \tag{13}$$

In the last step, it was once again used that cosine integrates to 0 over a whole period.

Unfortunately, the event plane is usually not known and hence there is no access to Ψ_{RP}. To remedy this, so called *two particle correlations* may be used. Denoting the angles of the tracks of the particles as ϕ_2 and ϕ_1, it follows that

$$\left\langle \cos(k(\phi_2 - \phi_1))\right\rangle = \left\langle \cos\left(k([(\phi_2 - \Psi_{\text{RP}}) - (\phi_1 - \Psi_{\text{RP}}]\right)\right\rangle \tag{14}$$

$$= \left\langle \cos[k(\phi_2 - \Psi_{\text{RP}})]\cos[k(\phi_1 - \Psi_{\text{RP}})] + \sin[k(\phi_2 - \Psi_{\text{RP}})]\sin[k(\phi_1 - \Psi_{\text{RP}})]\right\rangle. \tag{15}$$

Here, the subtraction formula for cosines has been used. Due to that the sine functions are odd around Ψ_{RP} their expectation value will evaluate to 0 in an infinite limit of the number of particles flowing out. In a case of lack of statistics, all the momentum could of course be carried by a single particle in one direction and many in another. If it is further assumed that ϕ_2 and ϕ_1 are independent from each other, it must be the case that

$$\left\langle \cos(k(\phi_2 - \phi_1)\right\rangle = \left\langle \cos[k(\phi_2 - \Psi_{\text{RP}})]\cdot\cos[k(\phi_1 - \Psi_{\text{RP}})]\right\rangle \tag{16}$$

$$= \left\langle \cos[k(\phi_2 - \Psi_{\text{RP}})]\right\rangle\left\langle \cos[k(\phi_1 - \Psi_{\text{RP}})]\right\rangle \tag{17}$$

$$= v_k \cdot v_k = v_k^2. \tag{18}$$

Conversely,

$$v_k = \sqrt{\left\langle \cos(k(\phi_2 - \phi_1) \right\rangle} \tag{19}$$

holds and in the special case of $k = 2$,

$$v_2 = \sqrt{\left\langle \cos(2(\phi_2 - \phi_1) \right\rangle} \tag{20}$$

where v_k has been taken as a positive quantity. This result gives that it is not necessary to compute Ψ_{RP} directly to know v_k.

There is however one issue with simply computing v_2 in this way and it relates to that the assumption of independent ϕ_2 and ϕ_1 is spoiled by effects such as jet production. Previous efforts to account for this has introduced arbitrary separations in values of η for which tracks are used to calculate the difference in φ when computing the expectation value in the above formula. See [13]. This to avoid including correlations between particles in the same jet, although not necessarily correlations for back to back jets. [7].

While such previous efforts have been able to calculate v_2 in many circumstances, the significant reduction in available data to perform statistical computations on has led to that v_2 has not been investigated in more peripheral collisions with larger centralities. The approach of this project is to try to account for this by studying the flow in proton on proton collisions (often abbreviated 'pp-collisions'), where there is no QGP, and accounting for that 'background' of non-flow QCD effects.

To do this, it may be assumed that the particle distribution, or rather two particle distribution as a function of $\Delta\varphi = \varphi_2 - \varphi_1$, is on the form

$$\frac{\mathrm{d}N^{\mathrm{Pb}}}{\mathrm{d}\Delta\varphi} = a \cdot \frac{\mathrm{d}N^{\mathrm{p}}}{\mathrm{d}\Delta\varphi} + b \cdot \left(1 + \sum_{k=1}^{\infty} 2\mathrm{v}_k \cos(k(\Delta\varphi)) \right). \tag{21}$$

Here, $\mathrm{d}N^{\mathrm{Pb}}$ is the (presumably small) number of particles that are associated with the angular difference $\Delta\varphi$ in the lead on lead collision (often abbreviated Pb-Pb collision). A similar interpretation holds for the first term on the right hand side (RHS) where 'p' stands for 'proton'. The motivation for writing the distribution on this form is that any periodic function may be described by a Fourier series. This time, the motivation for excluding sine-functions is that the difference $-\Delta\varphi$ should be equally likely as $\Delta\varphi$ as it is tantamount to changing the labels on φ_1 and φ_2. The transformation $\Delta\varphi \to -\Delta\varphi$ clearly has no effect on the cosine functions since they are even, while the sine functions lead to a change of sign as they are odd. Obviously, a physical observable cannot depend on how things are labelled. Note that the v_k here are not necessarily the same as the flow harmonics in equation (3). In this approach, the QCD 'background effects' are assumed to simply be scaled up linearly in larger collisions. A fit may be performed with the help of a computer program to find the various parameters in equation (21).

It is now necessary to relate the v_k to the v_k. This time, let

$$F(\varphi_2, \varphi_1) = 1 + \sum_{k=1}^{\infty} 2\mathrm{v}_k \cos(k(\Delta\varphi)). \tag{22}$$

By analogous steps to the derivation of equation (20), it follows that

$$\left\langle \cos(k\Delta\phi)\right\rangle = \frac{\int_0^{2\pi}\int_0^{2\pi} \mathrm{d}\phi_1\mathrm{d}\phi_2 \; F(\phi_1,\phi_2)\cos(k\Delta\phi)}{\int_0^{2\pi}\int_0^{2\pi} \mathrm{d}\phi_1\mathrm{d}\phi_2 \; F(\phi_1,\phi_2)} = ... = \tag{23}$$

$$= 2\mathrm{v}_k \frac{\int_0^{2\pi}\int_0^{2\pi} \mathrm{d}\phi_1\mathrm{d}\phi_2 \left(\frac{1}{2}+\frac{1}{2}\cos(2k\Delta\phi)\right)\Big)}{4\pi^2} \tag{24}$$

$$= 2\mathrm{v}_k \frac{2\pi^2}{4\pi^2} = \mathrm{v}_k. \tag{25}$$

Now, by equation (16), it holds that

$$\mathrm{v}_k = \left\langle \cos[k(\phi_2-\phi_1)]\right\rangle \tag{26}$$

$$= \left\langle \cos[k(\varphi_2-\Psi_{\mathrm{RP}})]\right\rangle\left\langle \cos[k(\varphi_1-\Psi_{\mathrm{RP}})]\right\rangle \tag{27}$$

$$= v_k \cdot v_k. \tag{28}$$

Hence,

$$\mathrm{v}_2 = v_2 \cdot v_2. \tag{29}$$

It should be kept in mind that this was derived under an assumption of only flow with no things such as jets to correlate φ_2 and φ_1 other than the flow. However, as v_2 is not actually calculated from an expectation value so this is not a problem. It is instead calculated from a fit to equation (21), which compensates for the non-flow effects.

4.8 The Purpose of the Forward Multiplicity Detectors

In order to increase the amount of available statistics, data may be taken from both the TPC and the FMD:s. Furthermore, correlating particles in the TPC and FMD:s may help reduce the probability of including intra-jet particle correlations in the data due to the different regions of η covered by the respective detectors. This is easily realised using equation (29) and its derivation. If two particle correlations are made with all different combinations of the TPC and FMD:s, it may be found that

$$\mathrm{v}_2^{\text{TPC-FMDA}} = \left\langle \cos[k(\phi^{\mathrm{TPC}}-\Psi_{\mathrm{RP}})]\right\rangle\left\langle \cos[k(\phi^{\mathrm{FMDA}}-\Psi_{\mathrm{RP}})]\right\rangle = v_2^{\mathrm{TPC}} \cdot v_2^{\mathrm{FMDA}}, \tag{30}$$

$$\mathrm{v}_2^{\text{TPC-FMDC}} = v_2^{\mathrm{TPC}} \cdot v_2^{\mathrm{FMDC}}, \tag{31}$$

and

$$\mathrm{v}_2^{\text{FMDA-FMDC}} = v_2^{\mathrm{FMDA}} \cdot v_2^{\mathrm{FMDC}}. \tag{32}$$

This is realised numerically by only taking difference between angles in the respective detectors when computing the distribution terms in equation (21). In order to compare with other measurements which may only involve the TPC, the value of v_2^{TPC} may be calculated to be

$$v_2^{\mathrm{TPC}} = \sqrt{\frac{\mathrm{v}_2^{\text{TPC-FMDA}} \cdot \mathrm{v}_2^{\text{TPC-FMDC}}}{\mathrm{v}_2^{\text{FMDA-FMDC}}}}. \tag{33}$$

Please note that the idea of measuring v_2 in this way is not my own but was given to me by my supervisor Vytautas Vislavicius.

A possible motivation for separately denoting a flow harmonic to belong to a specific detector is that the measured flow could differ for the different values of η which the detectors cover.

4.9 Event Mixing

One important aspect to consider with the FMD:s is their finite spatial resolution. This leads to that data is naturally 'histogrammed'. When calculating $\frac{\mathrm{d}N^{\mathrm{Pb}}}{\mathrm{d}\Delta\varphi}$ numerically, this will lead to that some differences are more likely to be obtained than others on a combinatorial basis. To make this clearer, imagine calculating $\Delta\varphi$ when both angles are taken from the same histogram. Let the histogram be over $[0, 2\pi)$ with a bin width of w. Clearly, there are many way to achieve the smallest possible value of $\Delta\varphi$, which in this case is w, by picking any neighbouring bins. On the contrary, there is only one way to achieve the maximum separation of $\Delta\varphi \approx 2\pi - 0 = 2\pi$ by combining the maximum and minimum bins' values. This effect leads to a bias with a preference to give higher 'counts' for some bin differences over others, and, even if the actual physical origin of the signal was completely isotropic, a stronger signal would still be observed for some $\Delta\varphi$ than others. Although in the case studied here, only the FMD:s have this issue of 'histogrammed data', it is still clear that this effect will be present anyhow. This combinatorial effect will also result in an uneven contribution from parts of the detectors with different $\Delta\eta$-values, which would lead to an unequal weighting of data.

This problem is commonly, as well as here, handled by *event mixing*. The procedure begins by first calculating the distribution $\frac{\mathrm{d}N^{\mathrm{Pb}}}{\mathrm{d}\Delta\varphi\,\mathrm{d}\Delta\eta}$ (which is essentially a two-dimensional histogram) as one would expect for all different events. Then, the same quantity may be calculated when i.e. φ_2 and η_2 are taken from one event and φ_1 and η_1 are taken from another such that the quantities are taken from different events. Note that it is necessary to perform this event-mixing on a per centrality interval basis to ensure that the events which are being mixed are comparable. If the total signal is computed from contributions from many unrelated events, the distribution of $\Delta\varphi$ and $\Delta\eta$ would be expected to be isotropic on average since there should be no physical signal present. This distribution may then, up to some normalisation factor, be interpreted as a probability density function for yielding an extra entry or 'count' in one bin even if the values of $\Delta\varphi$ and $\Delta\eta$ are random or taken from isotropic data. By dividing the intra-event correlations by a normalised event-mixing 'background', the combinatorial effects may be accounted for and 'unbiased' data may be acquired.

An added benefit of event mixing is that it takes into account other non-combinatorial effects such as detector (in)efficiencies because it gives what an isotropic distribution would result in. When dividing by this result, things like effector efficiencies are of course also taken into account by the 'probability density function'. Furthermore, since the elliptic flow is often given as a function of both transverse momentum p_T and the centrality, event mixing may be performed on a per momentum interval and per centrality interval basis. This may be necessary as detector efficiencies may also vary depending on particle momenta.

4.10 Statistical Uncertainties

Once the event mixing has been performed, the next step is to return to the form of $\dfrac{\mathrm{d}N^{\mathrm{Pb}}}{\mathrm{d}\Delta\varphi}$ as it is necessary when performing the fit to the model in equation (21). While this may of course be done by simply projecting the two-dimensional histogram to a one-dimensional one, this does not properly account for the uncertainties. If the errors in measurements are statistical in nature, a measurement of N counts is accompanied by an absolute uncertainty of $\delta N = \sqrt{N}$ and a fractional uncertainty of $\delta N/N = 1/\sqrt{N}$. If values corresponding to a given $\Delta\eta$ have a much smaller number of counts than others, the fractional statistical uncertainty is greater and that bin should presumably be weighted to a lesser extent than bins with smaller fractional uncertainties. To account for this, the formula for weighted averages

$$x_{\text{weighted average}} = \frac{\sum_i w_i x_i}{\sum_i w_i} \tag{34}$$

where $w_i = 1/\sigma_i^2$. Here, x_i are the measured values and σ_i their fractional statistical uncertainties. The fractional uncertainty of the weighted average is given by

$$\sigma_{\text{weighted average}} = \frac{1}{\sqrt{\sum_i w_i}}. \tag{35}$$

See Chapter 7 of [14] for a derivation.

Unfortunately, it is not as simple as simply plugging in $1/\sqrt{N_i}$ as the uncertainties. This is due to the fact that the statistical uncertainty in the event mixing also has to be accounted for, even if it could reasonably be assumed to be somewhat negligible due to there being more ways to mix angles in different events than to do intra-event correlations. If there are N_i counts in the 'raw' signal and M_i counts in the event mixing, the value $R_i \equiv N_i/M_i$ has its uncertainty given by the proper error propagation on the form

$$\frac{\delta R_i}{R_i} = \sqrt{\left(\frac{\delta N_i}{N_i}\right)^2 + \left(\frac{\delta M_i}{M_i}\right)^2} \tag{36}$$

$$= \sqrt{\frac{1}{N_i} + \frac{1}{M_i}}. \tag{37}$$

See chapter 3 of [14]. This is then what serves as the values of σ_i. Note that this averaging has to take place for each row in the two-dimensional 'histogram' $\dfrac{\mathrm{d}N^{\mathrm{Pb}}}{\mathrm{d}\Delta\varphi\,\mathrm{d}\Delta\eta}$ when the projection to the one-dimensional 'histogram' $\dfrac{\mathrm{d}N^{\mathrm{Pb}}}{\mathrm{d}\Delta\varphi}$ is performed.

Earlier, it was mentioned that the event mixing should be normalised. However, for the purposes of this report, it does not actually matter if the event mixing is normalised or scaled with any specific factor. The motivation for this being the case, as long as the uncertainties are properly propagated, is that when the fitting is done with respect to equation (21), there will be a degree of freedom in the scaling anyhow. Furthermore, this even introduces the freedom to scale the data by any factor at all, granted again that error propagation is properly performed to account for the scaling. Anyhow, the approach used here will be to

simply divide the entire event mixing by its maximum value such that the new maximum value is 1. This ensures that the order of magnitude stays roughly the same for the 'raw' histogram before and after the division.

This scaling may be desirable specifically for keeping the order of magnitude of the original data. If the scale is kept, then the data from both the proton-proton data and the lead on lead data may be divided by the number of tracks in the respective detectors to achieve a sort of normalisation w.r.t the number of tracks used to calculate the signal. Since this takes care of event mixing and accounts for the number of particles, and hence tracks, produced in the collision, the data sets should be roughly the same order of magnitude. This could help alleviate numerical instabilities when equation (21) is used in a fitting algorithm. It is important to keep in mind that error propagation must be performed if the event-mixing values in equation (36) have been changed by i.e. scaling them up or down by a constant factor.

Once the fit according to equation (21) has been done, it is of course of interest to know the uncertainty of the final values of v_2 (and hence also v_2^{TPC} through error propagation). Since the uncertainty δR_i is known for every 'bin' in the 'histogram' $\dfrac{\mathrm{d}N^{\mathrm{Pb}}}{\mathrm{d}\Delta\varphi}$, one could perform multiple fits do the data where each entry in the histogram has its value randomly changed according to a Gaussian distribution centred on R_i with a standard deviation of δR_i. The motivation for this is that the measured value has some deviation from the 'true' value it would have had in the case of infinite statistics. The deviation would then be given by a normal distribution. This random variation would of course be performed in both the proton on proton data and lead on lead data. From these various different fits, the mean and uncertainty could then be calculated according to

$$\bar{x} = \frac{1}{\#\text{Measurements}} \sum_i x_i \tag{38}$$

and

$$\delta\bar{x} = \sqrt{\frac{1}{\#\text{Measurements}} \sum_i (x_i - \bar{x})^2}. \tag{39}$$

Here, x_i are the measured values, $\bar{x}$ the mean value and '#' should be read as 'number of'.

5 Method

To be able to calculate the flow in lead-lead collisions, data taken in 2015 from the ALICE detector at CERN with a centre of momentum energy of $\sqrt{s_{NN}} = 5.02$ TeV was used for both lead on lead collisions and proton on proton collisions. In order to calculate the flow signals, the program ROOT on version 6.26, see [15], was used in conjunction with the programming language C++ to create many different two-dimensional histograms to hold data for various values of transverse momentum and various events of differing centralities. The used intervals for centralities were: 50% up to but not including 60%, 60% - 65%, 65% -70%, 70% - 75%, 75% -80%, 80% - 85% and 85% to 90% and the used intervals for the transverse momentum were, given in GeV, 0.2 up to but not including 0.5 GeV, 0.5 - 1.0, 1.0 - 1.5, 1.5 - 2.0, 2.0 - 2.5, 2.5 - 3.0, 3.0 - 3.5, 3.5 - 4.0, 4.0 - 5.0 and 5.0 - 6.0 GeV. The data used was stored in files created by ROOT using the 'TFile' class and stored with the help of the 'TTree' class

which had the structure as shown in Figure 7. Differences in values of the coordinates φ and η as defined in section 4.4 were then calculated for all measured tracks in different detectors assuming that they belonged to the intervals of $\eta \in [-0.75, 0.75]$ for the TPC or any of the intervals $[-3.1, -2]$, $[2.5, 3.1]$ or $[3.8, 4.7]$ in η for the FMD:s. The combinations of detectors used was the combinations of the TPC and the FMD with positive values of η, FMD1, the TPC and the FMD with negative values of η, FMD2, and the two FMD:s with differing signs of η. The values were always taken such that the first mentioned detector in the previous sentence had its value taken as the minuend and the latter had its value taken as the subtrahend. Depending on the centrality of the event, the differences were stored in different aforementioned histograms. Since values of transverse momentum were only available for tracks measured in the TPC, only combinations which included TPC-tracks were stored in separate histograms on a transverse momentum basis.

Following this, differences were calculated in the same way as previously described but with the tracks serving as minuend being taken from one event and the tracks serving as subtrahend being taken from another event. Such differences between previous events were calculated with five previous events for a given event and the results were stored in separate histograms such that the results could be used as event-mixing. All bins in the event-mixing histograms were then divided by the value of the 'bin' with the maximum number of 'counts' in their corresponding histograms. After these calculations had been performed, the histograms with the intra-event differences were divided on a per bin basis with their rescaled event-mixing counterparts. Values with 0 entries were ignored throughout this process to avoid dividing by 0. Throughout all of these scalings and divisions, uncertainties were propagated as described in the section 4.10.

In order to regain data usable when performing a fit according to equation (21), the histograms were projected into one-dimensional histograms with the help of equation (34). The corresponding uncertainty of each bin was also calculated.

Once all of the above had been done for the lead on lead collisions, this entire procedure was then repeated for the data containing the proton-proton collisions such that a fit according to equation (21) could be performed. The fit was then performed using the 'Fit()' member function of the ROOT class 'TH1D' using the Minuit2 fitter. Only the terms corresponding to the second and third flow harmonic in the summation sign in equation (21) were used in the fit. The fits were then performed multiple times when the values of the histograms' bins had been varied randomly, using the class 'TRandom2' with the seed '1', according to a normal distribution centred on each bins value with a standard deviation equal to each bin's previously calculated uncertainty. These different fit results were then used to calculate a mean value and an uncertainty for v_2. Equation (33) was then used to calculate the value of v_2^{TPC} and uncertainties were propagated. Finally, data which showed clear signs of not being correct was rejected from being used in the results. After the values had been calculated the computer code used was made available in **Annex 1**.

6 Results

It was possible to determine the values of v_2^{TPC} for centralities between 50% and 80% for the various values of p_T between 0.2 GeV up to 6 GeV. Beyond the centrality of 80%, the fits did not converge and the data began to visually deviate strongly from the form of other values. For the values that did converge, the values were roughly in-between the region of 0.05 to

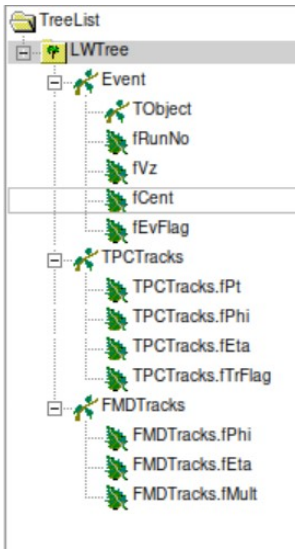

Figure 7: Shows an overview of the 'tree' in the program ROOT containing the measured values. For each 'branch' of the type 'Event', an array of various tracks of the type 'TPCTracks' and 'FMDTracks' was available containing the data. 'fPt' is the the transverse momentum and 'fCent' is the centrality of an event. 'fPhi', 'fEta' and 'fMult' stand for φ-values, η-values and multiplicity respectively.

0.35, see Figure 8a through Figure 8e. See Figure 14 for an example of when the data begins to visually deviate a lot. See Appendix 1 for a table with the calculated values of v_2.

The various plots for different values of transverse momentum p_T and centralities in lead on lead collisions showed, in general, a signal which closely resembled that of the term corresponding to v_2. For higher values of p_T, the measured corresponding proton on proton collision background began to show through more and more as expected. What is shown in Figure 9 and Figure 22 show qualitatively what both TPC-FMD1, TPC-FMD2 and FMD1-FMD2 correlations showed for low p_T-values. Figure 11 and Figure 15 show what, qualitatively, is measured in the signal from TPC-FMD1 and TPC-FMD2 correlations, with the peak at π growing more and more dominant for larger and larger values of p_T. Figure 10 and Figure 16 show the former cases of Figure 9 and Figure 15 but zoomed out such that the vertical axis starts at 0. Examples of proton-proton collision backgrounds are shown in Figure 13 and Figure 18.

The results for the FMD1-FMD2 correlations showed the same flow signal in lead-lead collisions as the other two cases for low values of p_T. However, the proton-proton background, which became larger and larger for higher centralities, was centred around 0 instead of π. See Figure 22 and Figure 19 for examples of the lead-lead signal beginning to resemble the proton-proton background as the centrality increases. See Figure 20 for the proton-proton background in the FMD1-FMD2 correlations.

Figure 12, Figure 17 and Figure 21 show examples of the lead-lead signal from other aforementioned figures having had the proton-proton background, scaled according to the constant found in the fit to equation (21), subtracted off. Finally, the amount of data which was processed in the end was roughly 147 GB of the lead-lead data and roughly 200 GB of proton-proton data. While the number of tracks varied from event to event, a rough estimate was that 73 MB corresponded to roughly 8842 events.

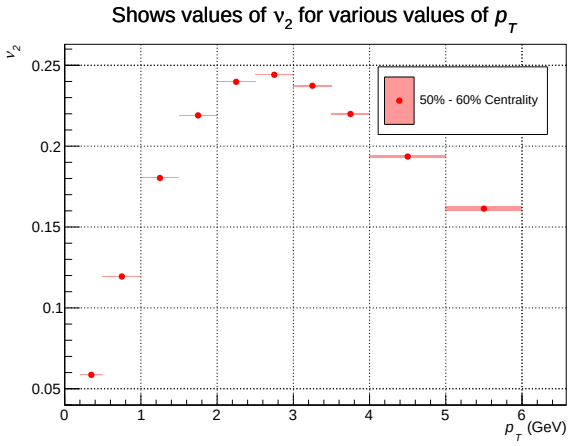

(a)

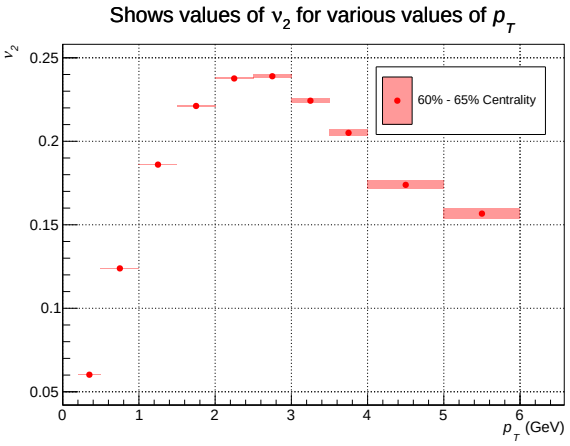

(b)

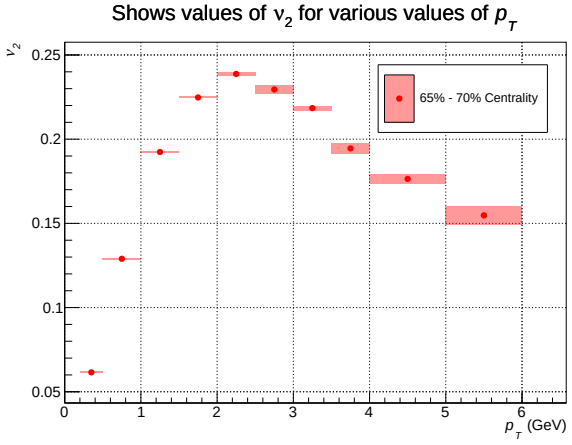

(c)

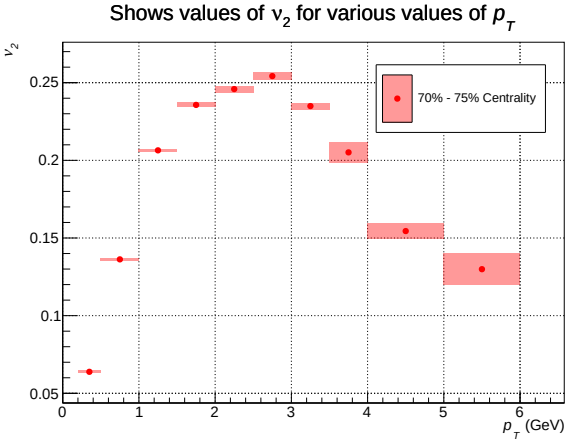

(d)

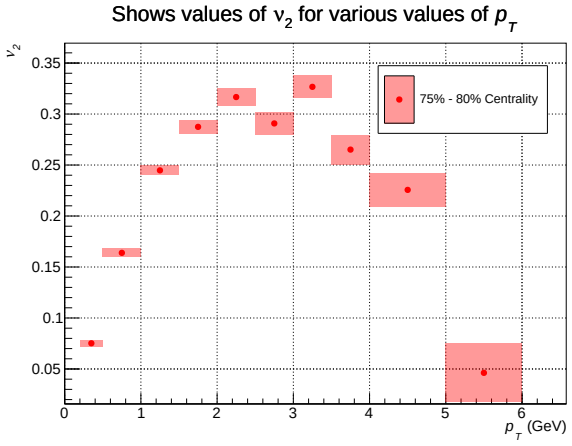

(e)

Figure 8: Shows measured values of v_2 for various regions of transverse momentum p_T. Each figure shows its own centrality interval and the given intervals are up to but not including the listed numbers.

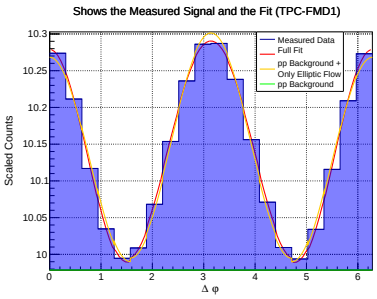

Figure 9: Shows an example of a fit for TPC-FMD1 data with a p_T-value in the interval 1.0 to 1.5 GeV and a centrality of 50% - 60% to equation (21) zoomed in to the top of the graph.

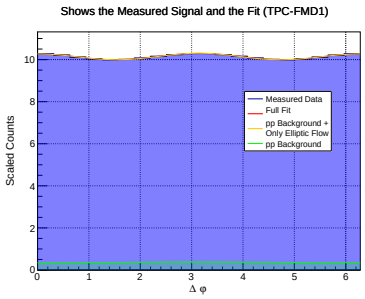

Figure 10: Shows the same data as in Figure 9 but zoomed out to make the proton-proton 'background' visible.

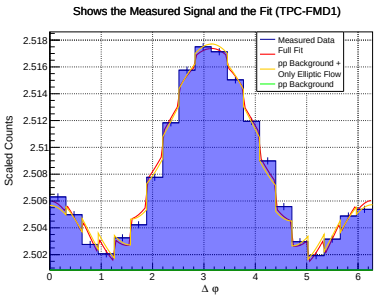

Figure 11:Shows an example of a fit for TPC-FMD1 data with p_T-value in the interval 0.2 to 0.5 GeV and a centrality of 75% - 80% to equation (21) zoomed in to the top of the graph.

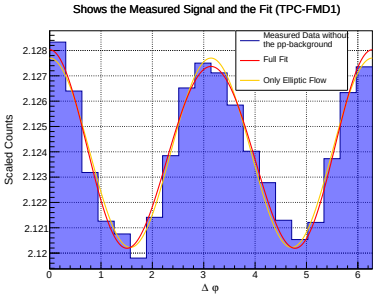

Figure 12: Shows the same data as in Figure 11 but with the proton-proton background scaled by the fit result of equation (21) subtracted off both the data and the red and orange fit lines.

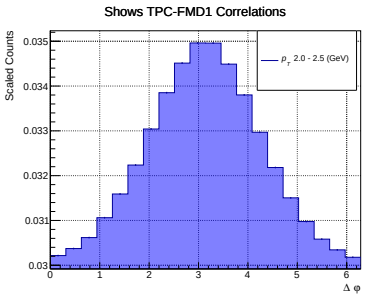

Figure 13: Shows an example of a proton-proton background for the p_T interval 2.0 to 2.5 GeV

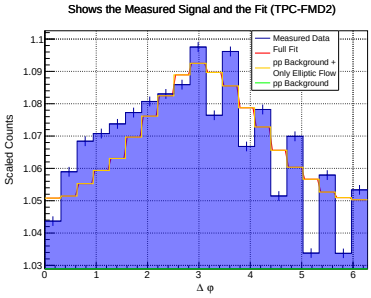

Figure 14: Shows an example of when the measured data begins to deviate a lot from other measurements for large centralities. This is for the p_T-interval 2.0 to 2.5 GeV and the centrality interval 85% to 90%.

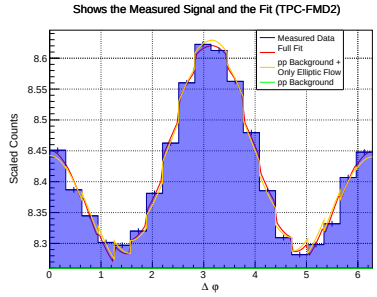

Figure 15: Shows an example of a fit for TPC-FMD2 data with p_T-value in the interval 3.0 to 3.5 GeV and a centrality of 65% - 70% to equation (21) zoomed in to the top of the graph.

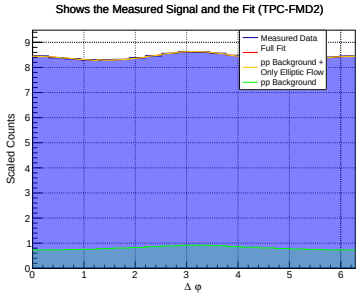

Figure 16: Shows the same data as in Figure 15 but zoomed out to make the proton-proton 'background' visible.

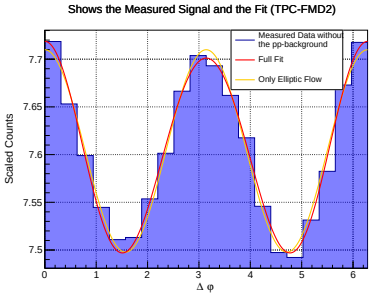

Figure 17: Shows the same data as in Figure 15 but with the proton-proton background scaled by the fit result of equation (21) subtracted off both the data and the red and orange fit lines.

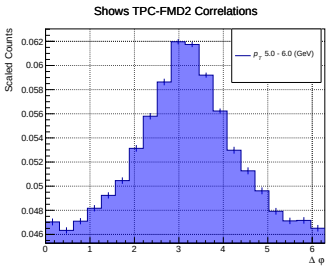

Figure 18: Shows an example of a proton-proton background for the p_T interval 5.0 to 6.0 GeV.

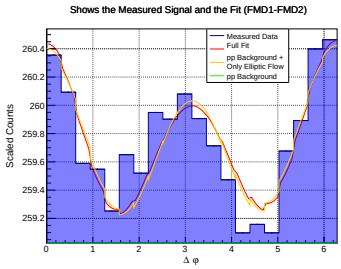

Figure 19: Shows an example of FMD1-FMD2 correlations in the centrality interval 65% to 70%.

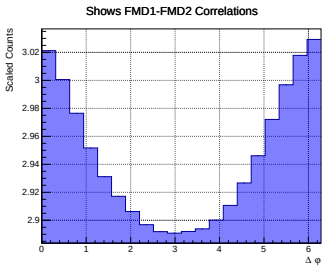

Figure 20: Shows the proton-proton background for the FMD1-FMD2 correlations.

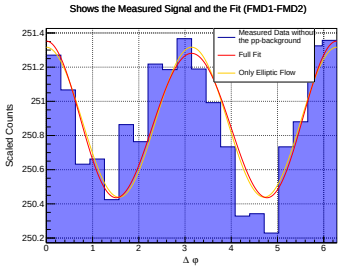

Figure 21: Shows the same data as in Figure 19 but with the proton-proton background scaled by the fit result of equation (21) subtracted off.

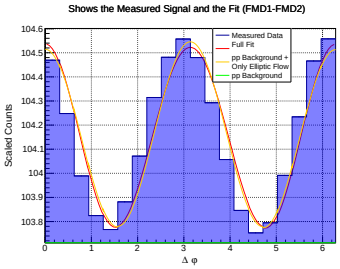

Figure 22: Shows an example of FMD1-FMD2 correlations in the centrality interval 50% to 60%.

7 Discussion

It may be concluded that it was possible to measure v_2 in high centrality regions of data. The data in Figure 8 seems to show a somewhat distorted parabola in terms of the measured values with a peak in elliptic flow between 2 GeV and 3 GeV. If Figures 9, 11 and 13 are viewed (or Figure 15 and Figure 18 for that matter), it is clear that the non-flow effects present in proton on proton collisions begin to assert themselves for higher centralities and higher values of p_T. From Figure 12, Figure 17 and Figure 21 it is also clear that these non-flow effects correspond very well to the scaled up proton on proton background as the subtraction performed in those figures returns the original shape. Furthermore, since all of these figures show both the data and the fit lines having had the proton on proton background subtracted off, and since these fits are clearly continuous, this clearly indicates that the 'kinks' in the fits of the original figures are solely caused by the discrete steps of the proton on proton background included in the fits of the original figures. The growing peak around π is of course expected as the particles in jets tend to be very energetic and hence have a high transverse momentum, while a higher centrality of course means that fewer nucleons actually interact to generate flow. This also seems to indicate that the assumption that the non-flow effects from QCD scaling up linearly in equation (21) was valid. Furthermore, if the data from Figure 8 is compared to previous results, such as Figure 5 in [13], it is clear that the somewhat stretched out parabolic shape agrees with previous measurements. Furthermore, the order of magnitude also seems to be similar. However, due the larger intervals of p_T used in the calculations of Figure 8 in this report, some results may not be directly comparable.

As for the fitting itself, this seems to work fairly well as seen in Figure 9, Figure 11, Figure 15, Figure 19 and Figure 22. One aspect of these fits is that only the terms corresponding to

v_2 and v_3 were used in the fit according to equation (21). While this might in theory provide a lesser quality fit as the contribution for higher order terms are neglected, it is clear from Figure 9, Figure 11, Figure 15, Figure 19 and Figure 22 when looking at the orange line and the red line that almost all of the contribution comes from the term corresponding to v_2. This clearly means that any such effects would be small. While this could of course easily be solved by including more terms, this would come with its own set of issues. Primarily, the issue with using a complete Fourier series is that any measured signal, even one with no v_2 signal at all, would give a very good fit since any reasonable periodic physical signal may be represented in this way. If only the first few terms are used and there is not much of v_2 in the signal, this will quickly become apparent in the vertical error bars of Figure 8 as the random small changes in v_2 could cause, at least in terms of percentages, a very large difference in v_2. It would hence become apparent immediately if the fit was bad this way. Furthermore, using too many free parameters might cause numerical instabilities when performing the fit.

Clearly, some of the fitting results failed for higher centralities. This was likely caused by a lack of data. The results of i.e. Figure 14 were common during testing of the code when only small data samples were used to get quick results. It was quickly apparent during this testing that a very large data sample was necessary to actually see the signal. While the small error bars in Figure 14 may seem to dispute this, that does not have to be the case. It was clear throughout testing that the actual signal as seen in i.e. Figure 9, Figure 11, Figure 15, Figure 19 and Figure 22 were tiny fluctuations added onto the background which consisted combinatorial effects which event mixing took care of later on. Clearly, if the number of tracks in a given event are few, the available statistics for the event mixing to 'do mixing on' by combining tracks becomes small. On the other hand, the raw signal would not necessarily suffer from a lack of statistics due to the many events. If this is indeed the cause, a solution for this would had been to have done event mixing with more previous events for events with higher centralities and larger values of p_T.

Another apparent strange thing is the result of the proton on proton background in Figure 20. Obviously, one would expect a peak at π and not around 0. While this could be considered an error in the data processing, this does not necessarily have to be so. Since the data for low centralities in the FMD1-FMD2 correlations looked qualitatively as Figure 9, which may be seen from Figure 22, and then begins to have the shape of Figure 20 imposed on the data for higher centralities (as seen in Figure 19), this clearly shows that it is not the case that this signal is present only in the proton on proton background. Furthermore, since it runs on the exact same code and manages to produce the expected output for the lower centrality events, this also suggest that the error might not be with the code. One possible physical explanation for the origin of this signal could be related to the geometry. If the surface area of the cone of a jet is much larger than the surface area of an FMD, only a small fraction of the particles in a jet might be detected. Hence, only the particles with the very highest values of η would contribute and the back to back jets would definitely have a correlation. Another possible explanation is the much fewer available tracks in the FMD:s, which as discussed earlier, could result in a problem with accounting for combinatorial effects in the event mixing. A valid solution would then be to increase the number of previous events that event mixing is performed for when doing event mixing for FMD1-FMD2 correlations. This would also explain why the peak is around 0 as discussed in the section 4.9.

One observation that may be made from Figure 19 and Figure 22 is that the fit lines are

slightly shifted to the right compared to the experimental data. Since the elliptic flow is even around π, the fits according to terms of equation (21) are of course centred around π and the experimental data is hence centred on a value which by eye seems to be closer to 3. A likely reason for this is due to the binning. As may be seen in the mentioned figures, there are clearly 20 bins present over the interval of $[0, 2\pi)$. These bins were chosen due to the FMD:s having 20 discrete φ-values available. This places the edge between the two central bins right at π. Since the values of the TPC are continuous, this would of course not cause any problems for the TPC-FMD1 and TPC-FMD2 correlations since the fluctuations around π would average out due to the continuous nature. For the FMD1-FMD2 correlations, this might not happen as easily as both of the chosen angles would belong to a discrete set of values. This would then explain why the data is shifted slightly. A possible way to resolve this issue is to simply shift the interval the data is plotted over with some value δ such that the interval becomes $[0 + \delta, 2\pi + \delta)$. Doing this would cause values of π to fall distinctively into one bin and not occur between the edges of two bins.

Additionally, it should be mentioned that some data was rejected during the data processing. While inspecting the results, it was clear that one data set for the proton on proton data showed an asymmetric result which could be discarded on the grounds of momentum conservation. Data sets with different cutting options for the same events were then investigated and the data set which corresponded to the previously asymmetric one showed exactly the same asymmetry, while the others did not. On these grounds it was assumed that something about that actual data set was not correct and the judgement was made to reject this data.

In conclusion, it may be stated that it was possible to investigate very peripheral high centrality events and determine the elliptic flow using the approach of this project and the proton on proton background definitely seemed to be superimposed on the flow signal.

8 Outlook

While the results were definitely enough to comply with the set out goal, there are still many improvements which can be made. One such improvement would be the previously discussed increase in number of previous events that event mixing was with in cases where there was less available statistics. Another possible improvement would be to account for slight shifts along the beam line of which collisions took place. Throughout this document, it has been assumed that the collisions take place at exactly the centre of the detector. This does not necessarily have to be the case. As the data for these shifts are available, see the 'leaf' called 'fVz' on the 'Event' branch in Figure 7, a three-dimensional histogram could had been used instead of a two-dimensional one to perform the event mixing to take this into account. However, since some failures of results were previously discussed to likely be due to a lack of statistics, this would of course come with the problem of reducing the amount of available statistics. If more time had been available or if access to a super computer had been present, the data could of course had been analysed in smaller p_T intervals to make the data more comparable to the results of Figure 5 in [13].

One possible improvement to solve the issue of lack of statistics for event mixing would be to take an analytical approach to the combinatorial effects in the 'histogramming'. Clearly, the combinatorial effects are a property that arise solely from the histograms' binning and not from the actual physical signal. If nested `for`-loops are used to loop through each entry of histograms with one entry in every bin once, to then calculate the bin difference for every

possible combination of bins, and one then adds the counts to an 'event-mixing' histogram, this combinatorial effect could be entirely accounted for. Even if the data from the TPC is not histogrammed, data is always associated with uncertainty which could be used to 'histogram it' (that is to say that $a = 1.00$ technically means that $a \in [0.995, 1.005)$). This would clearly only have to be performed once in total and not once per histogram. Since event mixing takes a lot longer than the normal computation of the raw signal, this could speed up the computation process considerably.

The reason for this not being done here is that it does not account for varying detector efficiencies which may both vary in space, but also be different for particles with different momenta. The detector efficiencies could also possibly degrade over time depending on the materials used in the detector. However, if more intricate knowledge of the detector had been reasonable to gain during an allotted time span, these effects could also had been accounted for. Even if the 'efficiency bias' had to be updated for subsequent series of runs of the detector to account for material degradation, it would still not need to be done for every possible combination of track and would hence save a lot of computation time. Unfortunately, calculating what φ- and η-values would be expected from an isotropic signal would require taking into account more specific knowledge of the geometry of the detector. Since the event-mixing is what takes the most time, and would also go up to $\mathcal{O}(n^3)$ if 'fVz' was accounted for, this could certainly allow for the processing of more statistics much faster.

9 References

[1] G. Kane, *Modern elementary particle physics, Explaining and extending the standard model*, second edition (Cambridge University Press, 2017).

[2] B. R. Martin and G. Shaw, *Particle physics*, third edition (John Wiley & Sons Ltd, 2008).

[3] W. Florkowski, *Phenomenology of ultra-relativistic heavy-ion collisions* (World Scientific Publishing Co. Pte. Ltd., 2010).

[4] E. Avsar, Y. Hatta, C. Flensburg, J. Y. Ollitrault, and T. Ueda, "Eccentricity and elliptic flow in pp collisions at the LHC", J. Phys. G **38**, edited by Y. Schutz and U. A. Wiedemann, 124053 (2011).

[5] K. Aamodt et al. (ALICE), "The ALICE experiment at the CERN LHC", JINST **3**, S08002 (2008).

[6] The ALICE website used on May 12$^{\text{th}}$ 2023, `https://alice-collaboration.web.cern.ch/node/34960`.

[7] Information given to me by my supervisor Vytautas Vislavicius.

[8] G. Barr, R. Devenish, R. Walczak, and T. Weidberg, *Particle Physics in the LHC Era* (Oxford University Press, Jan. 2016).

[9] J. Lilley, *Nuclear physics, Principles and applications* (John Wiley & Sons Ltd, 2001).

[10] B. Abelev et al. (ALICE), "Centrality determination of Pb-Pb collisions at $\sqrt{s_{NN}} = 2.76$ TeV with ALICE", Phys. Rev. C **88**, 044909 (2013).

[11] P. Christiansen, "Kvark-gluon plasmaet – den perfekte væske vi ikke kan forstå", KVANT – Tidsskrift for Fysik og Astronomi.

[12] B. V. Jacak and B. Müller, "The exploration of hot nuclear matter", Science **337**, 310–314 (2012).

[13] The fifth figure on the ALICE website used on May 12$^{\text{th}}$ 2023, `https://alice-publications.web.cern.ch/node/4287`.

[14] J. R. Taylor, *An introduction to error analysis, The study of uncertainties in physical measurements*, second edition (University Science Books, 1997).

[15] Version 6.26 of the ROOT Data Analysis framework
from CERN, available at `https://root.cern/install/all_releases/`.

Appendix A - Table of v_2-values

Table 1: Shows the measured values of v_2 for various intervals of centralities and transverse momenta p_T as well as the calculated uncertainties.

p_T Interval	$50\% - 60\%$ Centrality	$60\% - 65\%$ Centrality	$65\% - 70\%$ Centrality	$70\% - 75\%$ Centrality	$75\% - 80\%$ Centrality
$0.2 - 0.5$ GeV	$0.0585892 \pm 8.58332 \cdot 10^{-5}$	$0.0602192 \pm 0.000178192$	$0.0615192 \pm 0.000334362$	$0.0638396 \pm 0.000723565$	0.0752155 ± 0.00311788
$0.5 - 1.0$ GeV	$0.119427 \pm 9.12242 \cdot 10^{-5}$	0.123888 ± 0.000242741	0.128965 ± 0.000364806	0.136237 ± 0.000876439	0.163877 ± 0.00424407
$1.0 - 1.5$ GeV	$0.180332 \pm 8.12503 \cdot 10^{-5}$	0.186034 ± 0.000266943	0.192378 ± 0.000403626	0.206436 ± 0.00076728	0.244768 ± 0.00445663
$1.5 - 2.0$ GeV	0.219028 ± 0.000145249	0.221148 ± 0.000455179	0.224766 ± 0.000494497	0.23569 ± 0.00135693	0.287422 ± 0.00681581
$2.0 - 2.5$ GeV	0.239767 ± 0.000135129	0.237619 ± 0.000454429	0.23873 ± 0.000988537	0.245897 ± 0.00199781	0.316659 ± 0.00867926
$2.5 - 3.0$ GeV	0.244124 ± 0.000256812	0.238956 ± 0.0011189	0.229517 ± 0.00251999	0.254247 ± 0.00244792	0.290783 ± 0.0108699
$3.0 - 3.5$ GeV	0.237355 ± 0.000311634	0.224298 ± 0.00132156	0.218454 ± 0.00131625	0.234942 ± 0.00217096	0.326668 ± 0.0108408
$3.5 - 4.0$ GeV	0.219884 ± 0.000603763	0.205042 ± 0.00206822	0.194516 ± 0.00299939	0.205129 ± 0.00655752	0.265119 ± 0.0145923
$4.0 - 5.0$ GeV	0.193574 ± 0.000663706	0.173905 ± 0.00240071	0.17642 ± 0.0027742	0.154459 ± 0.00486404	0.225625 ± 0.016656
$5.0 - 6.0$ GeV	0.161361 ± 0.00124006	0.156688 ± 0.0031197	0.154756 ± 0.00555929	0.129918 ± 0.0102898	0.0462025 ± 0.0287235